Society of Medical Education & Research

2025, Volume 5, Issue 1, Page No: 18-39

ISSN: 3108-4834

Archive of International Journal of Cancer and Allied Science

UBE2J1 Suppresses Colorectal Cancer Progression via Ubiquitin-Mediated Degradation of RPS3

Diego Sebastian Rivas[1]*, Pablo Andres Molina[1]

[1]Department of Oncology, Universidad Nacional de Rosario, Rosario, Argentina.

***E-mail** ✉ d.rivas.unr@gmail.com

Abstract

Ubiquitin-conjugating enzyme E2 J1 (UBE2J1) has been shown to be involved in the ubiquitination of various substrate proteins; however, its mechanistic role in cancer initiation and progression remains poorly understood. In this study, we demonstrate that UBE2J1 expression is significantly reduced in colorectal cancer (CRC) tissues and cell lines as a consequence of promoter DNA hypermethylation, and that low UBE2J1 levels are correlated with unfavorable clinical outcomes. Functional analyses reveal that UBE2J1 acts as a tumor suppressor, markedly inhibiting CRC cell proliferation and metastatic potential. Mechanistically, UBE2J1 forms an E2–E3 ubiquitination complex with TRIM25, which directly interacts with ribosomal protein S3 (RPS3) and promotes its ubiquitination and proteasomal degradation at lysine 214. The resulting reduction in RPS3 levels impairs nuclear translocation of NF-κB, thereby suppressing activation of the NF-κB signaling pathway. Collectively, our findings uncover a previously unrecognized mechanism whereby UBE2J1-mediated polyubiquitination and degradation of RPS3 disrupts NF-κB signaling, highlighting UBE2J1 as a potential prognostic biomarker and therapeutic target in CRC.

Keywords: Colorectal cancer, UBE2J1, Ribosomal protein, Nuclear translocation

Introduction

Colorectal cancer (CRC) constitutes a major cause of cancer morbidity and mortality worldwide, ranking third in global incidence and second in cancer-related deaths [1]. In 2020, CRC accounted for approximately 1.9 million new cases and nearly 935,000 deaths globally [2]. Although treatment modalities such as surgical resection, radiotherapy, chemotherapy, targeted therapy, and immunotherapy have markedly improved patient management, individuals diagnosed with advanced CRC continue to experience unfavorable clinical outcomes [3, 4]. These challenges underscore the necessity of defining the molecular mechanisms that underlie CRC progression and metastatic spread, which may facilitate the discovery of effective biomarkers and innovative therapeutic targets.

The ubiquitin–proteasome system (UPS) is the principal mechanism responsible for regulated protein degradation in eukaryotic cells [5, 6]. Protein ubiquitination is orchestrated through the sequential actions of ubiquitin-activating enzymes (E1), ubiquitin-conjugating enzymes (E2), and ubiquitin ligases (E3), which together catalyze the attachment of ubiquitin moieties to target proteins [7, 8]. Accumulating evidence indicates that aberrations in the UPS contribute to multiple oncogenic processes, including dysregulated cell cycle progression, angiogenesis, tumor cell proliferation, migration, invasion, and metastasis [9-11]. Ubiquitin-conjugating enzyme E2 J1 (UBE2J1), a member of the E2 enzyme family, is localized to the endoplasmic reticulum (ER) membrane and consists of a luminal region, a single transmembrane domain, and a cytosolic catalytic domain [12]. Previous studies have demonstrated that UBE2J1 participates in the ubiquitination and degradation of

Access this article online https://smerpub.com/

Received: 18 November 2024; **Accepted:** 27 February 2025

How to cite this article: Rivas DS, Molina PA. UBE2J1 Suppresses Colorectal Cancer Progression via Ubiquitin-Mediated Degradation of RPS3 Arch Int J Cancer Allied Sci. 2025;5(1):18-39. https://doi.org/10.51847/7UbioAJLAO

diverse substrate proteins. For example, UBE2J1 associates with the c-IAP1/TRAF2 complex to enhance TRAF2 ubiquitination [13]. In addition, UBE2J1 cooperates with the E3 ligase HRD1 to mediate the proteasomal degradation of misfolded major histocompatibility complex class I (MHC I) molecules [14], and functions together with Derlin-1 and RMA1 to promote the degradation of aberrant cystic fibrosis transmembrane conductance regulator (CFTR) proteins [15]. Collectively, these findings highlight the central role of UBE2J1 in ER-associated protein degradation (ERAD). Moreover, UBE2J1 has been shown to facilitate the ubiquitination of interferon regulatory factor 3 (IRF3), thereby suppressing type I interferon production and enhancing RNA virus infection [16]. Despite these insights, the biological significance of UBE2J1 in cancer remains insufficiently investigated [17-19].

Nuclear factor κB (NF-κB) is a multifunctional transcription factor that plays a crucial role in tumor development and progression [20, 21]. Persistent activation of NF-κB signaling has been widely linked to enhanced tumor cell proliferation, angiogenesis, resistance to therapy, and metastatic capacity [22, 23]. Ribosomal protein S3 (RPS3) is a structural component of the 40S ribosomal subunit and interacts with eukaryotic initiation factors eIF2 and eIF3 to regulate translation initiation and ribosome maturation [24]. Beyond its canonical role in protein synthesis, RPS3 exerts a range of extra-ribosomal functions, including involvement in DNA repair, apoptosis, and cellular responses to radiation [25-27]. Notably, radiation-induced dissociation of the macrophage migration inhibitory factor (MIF)–RPS3 complex has been reported to activate NF-κB signaling, thereby promoting proliferation, inflammation, and metastasis in non–small cell lung cancer (NSCLC) [28]. Importantly, RPS3 can act as a non-Rel subunit of the NF-κB complex by directly interacting with the p65 subunit through its K homology (KH) domain, thereby enhancing NF-κB–dependent transcriptional activity [29]. However, the mechanisms regulating RPS3 expression and function in CRC remain poorly defined.

In this study, we report that UBE2J1 expression is significantly reduced in CRC as a result of promoter hypermethylation, and that decreased UBE2J1 levels are associated with poor patient prognosis. Functional experiments demonstrate that UBE2J1 suppresses CRC cell proliferation and metastatic potential both in vitro and in vivo. Mechanistically, UBE2J1 forms a functional E2–E3 complex with TRIM25, which directly targets RPS3 for ubiquitination and proteasomal degradation at lysine 214. The consequent reduction in RPS3 levels limits NF-κB nuclear translocation, thereby attenuating NF-κB signaling activity.

Results and Discussion

Reduced UBE2J1 expression in colorectal cancer correlates with disease aggressiveness and patient outcome

To uncover proteins associated with colorectal cancer (CRC) progression, comparative proteomic analysis was carried out using paired adjacent normal tissue, primary tumor samples, and corresponding liver metastases collected from three CRC patients (**Figure 1a**). Differential protein expression profiling identified a subset of markedly altered proteins, which were visualized as the top 20 upregulated and downregulated candidates in a heatmap. These candidates were further assessed by qRT-PCR in an independent set of 24 matched tissue pairs **(Figures 1a and 1b).** Among the validated genes, UBE2J1 showed the most pronounced reduction in expression and was therefore selected for in-depth analysis.

To systematically evaluate the clinical relevance of UBE2J1, its expression was examined at both transcript and protein levels in CRC patient cohorts. Quantitative RT-PCR analysis was performed on 200 tumor samples (cohort 1), while protein expression was assessed using western blotting in 9 paired samples and immunohistochemistry (IHC) in 50 CRC cases (cohort 2). These analyses consistently demonstrated a significant decrease in UBE2J1 expression in CRC tissues compared with adjacent non-tumorous counterparts (**Figure 1b**). Moreover, UBE2J1 protein abundance was lowest in metastatic lesions, intermediate in primary tumors, and highest in adjacent normal tissues (**Figure 1c**).

Correlation analysis revealed that diminished UBE2J1 mRNA expression was significantly associated with more aggressive clinicopathological features, including larger tumor size ($P = 0.0067$), advanced T stage ($P = 0.0353$), higher TNM stage ($P = 0.0024$), lymph node involvement ($P = 0.0125$), and distant metastasis ($P = 0.0112$) **(Table 1)**. These findings imply a potential suppressive role for UBE2J1 in CRC tumor growth and dissemination. Immunohistochemical staining further confirmed markedly weaker UBE2J1 signals in tumor

tissues compared with adjacent normal tissues, with predominant localization observed in the cytoplasm (**Figures 1d and e**).

Prognostic evaluation using Kaplan–Meier survival curves demonstrated that patients with reduced UBE2J1 protein expression had significantly shorter overall survival than those with higher expression levels (**Figure 1f**). Consistently, analyses of external datasets from The Cancer Genome Atlas (TCGA) and the Gene Expression Omnibus (GEO; GSE41258) validated the decreased expression of UBE2J1 in CRC tissues and revealed a positive association between elevated UBE2J1 expression and improved recurrence-free survival (RFS) and overall survival (OS) (**Figures 1g–k**). Together, these results indicate that loss of UBE2J1 expression is closely linked to CRC progression and poor clinical outcomes, supporting its potential utility as a diagnostic and prognostic biomarker.

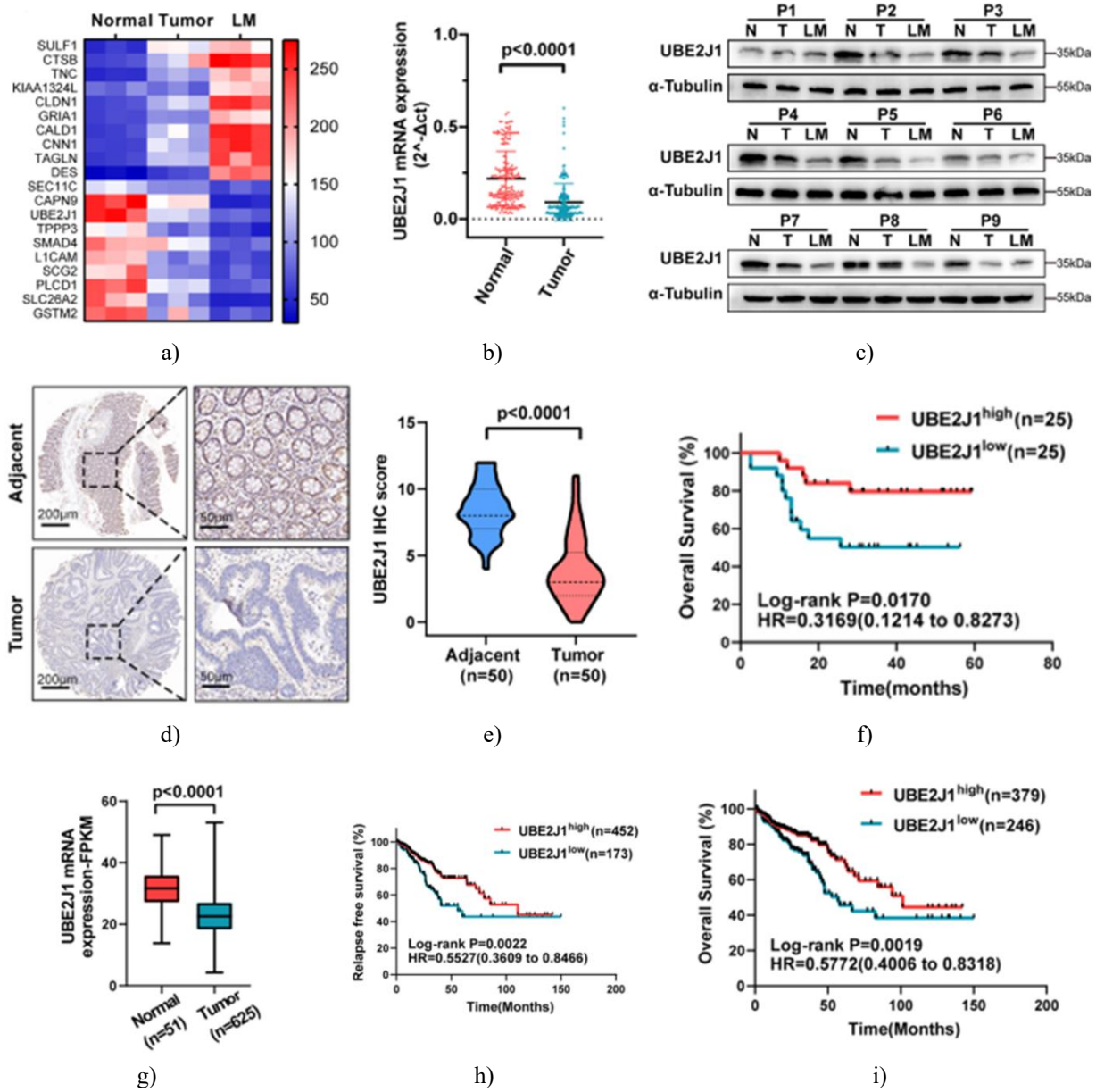

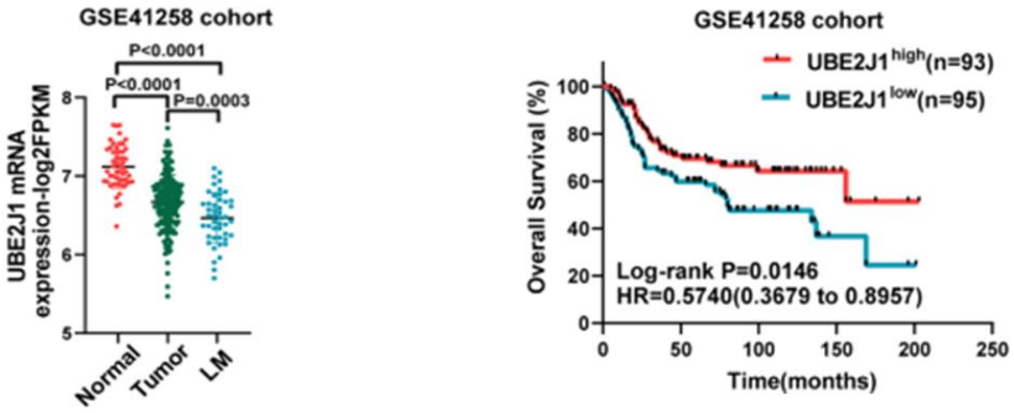

j) k)

Figure 1. Reduced expression of UBE2J1 in colorectal cancer and its link to better patient outcomes

(a) A heatmap illustrating the 20 most significantly up- and downregulated proteins across paired samples of liver metastases (LM), primary tumors, and nearby healthy tissue from three individuals with colorectal cancer (CRC). **(b)** Assessment of UBE2J1 mRNA levels using quantitative real-time PCR in 200 paired CRC tumor samples and adjacent normal colorectal tissues (from cohort 1). **(c)** Evaluation of UBE2J1 protein abundance by Western blot analysis in nine paired sets of liver metastases, primary tumors, and matching normal tissues. **(d–f)** Immunohistochemistry (IHC) examination of UBE2J1 protein in 50 paired CRC tumors and adjacent normal samples (cohort 2): **(d)** Example images of IHC staining for UBE2J1. **(e)** Scoring and quantification of IHC staining intensity. **(f)** Kaplan-Meier curves for survival, dividing patients into groups with low (n=25) or high (n=25) UBE2J1 expression. **(g)** Analysis of UBE2J1 gene expression data from The Cancer Genome Atlas (TCGA) CRC dataset. **(h, i)** Survival plots (relapse-free and overall) based on UBE2J1 levels in the TCGA CRC patient group. **(j)** UBE2J1 expression profile in the GSE41258 CRC dataset. **(k)** Kaplan-Meier analysis of overall survival stratified by UBE2J1 expression in the GSE41258 cohort.

Data are shown as mean ± standard deviation from triplicate experiments; statistical significance was set at $P < 0.05$.

Epigenetic inactivation of UBE2J1 via promoter CpG Island methylation in colorectal cancer

As UBE2J1 appears to function as a tumor suppressor, we explored the reasons for its reduced expression in CRC. Analysis of the UBE2J1 promoter using bioinformatics tools identified a typical CpG island (**Figure 2a**), suggesting that epigenetic modifications, specifically DNA methylation, might silence the gene.

Semi-quantitative reverse transcription PCR revealed strong UBE2J1 expression in the normal colon epithelial cell line NCM460, varying degrees of reduced expression in CRC lines such as SW620, SW480, Caco-2, and HT-29, and complete absence in HCT 116 cells. Exposure to the demethylating agent 5-aza-2'-deoxycytidine (5-Aza) restored UBE2J1 expression in those cell lines with low or no baseline levels (**Figure 2b**).

Methylation-specific PCR (MSP) detected complete methylation of the promoter in HT-29 and HCT 116 cells, partial methylation in LoVo, DLD-1, SW480, SW620 and Caco-2 cells, and no methylation in NCM460 cells (**Figure 2c**). These findings were validated through bisulfite genomic sequencing in representative lines (LoVo, HT-29, DLD-1, and HCT 116; **Figure 2d**).

In patient samples, MSP analysis revealed UBE2J1 promoter methylation in 71.4% (20 out of 28) of primary CRC tumors, while no methylation was observed in any of the 28 paired normal adjacent tissues (**Figure 2e**).

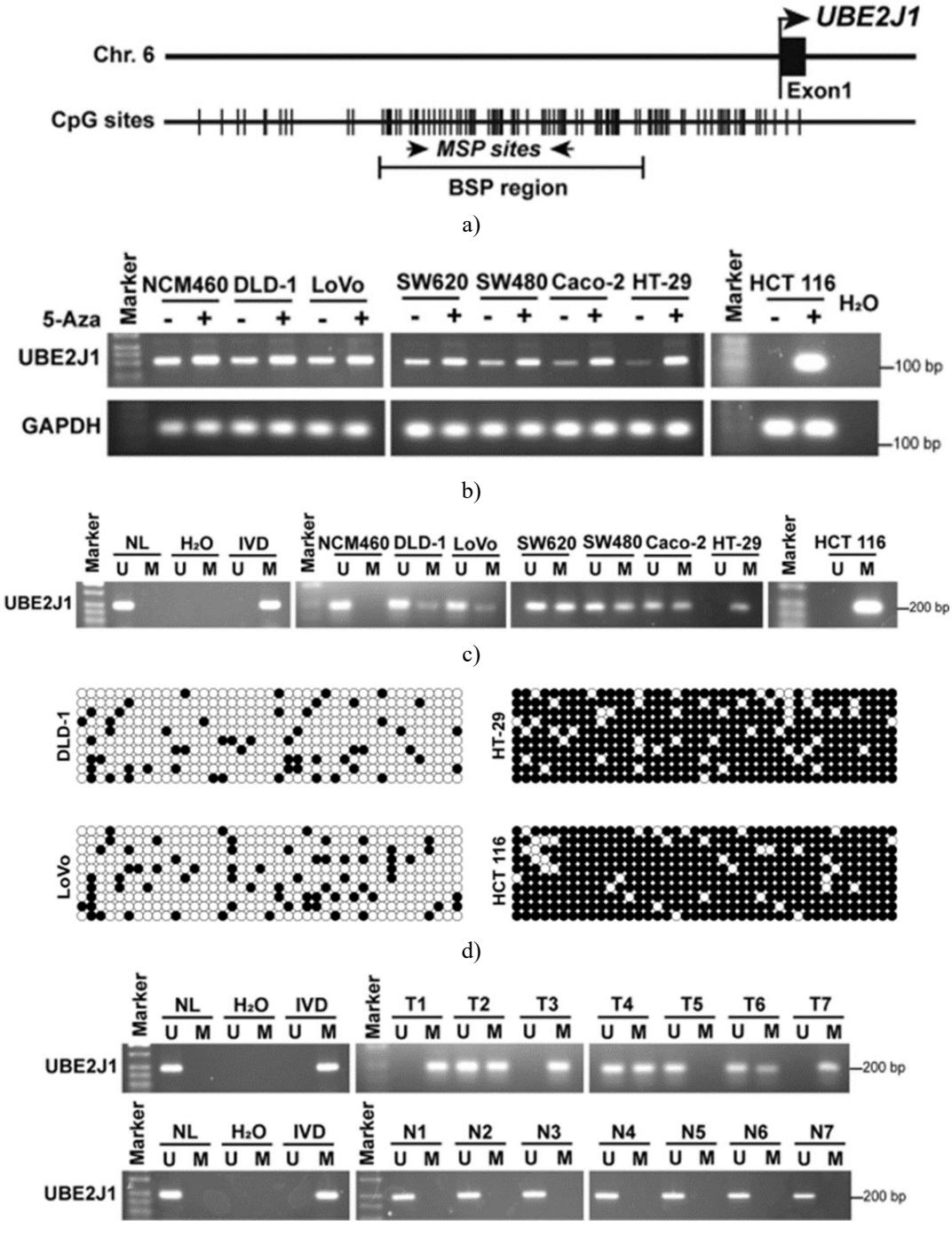

Figure 2. UBE2J1 is silenced by promoter CpG methylation in colorectal cancer

a The UBE2J1 promoter harbors a canonical CpG island. The diagram highlights the CpG sites, the regions analyzed by MSP, and the sequences assessed with BSP. **b** Semi-quantitative RT-PCR was used to measure UBE2J1 expression in normal colonic epithelial cells and seven CRC cell lines, both with and without treatment with the demethylating agent 5-aza-2′-deoxycytidine (5-Aza). In untreated cells, UBE2J1 expression was absent or reduced in several CRC lines but was restored following 5-Aza exposure. H_2O served as a negative control, and GAPDH was used as a normalization reference. **c** MSP analysis confirmed the methylation

status of the UBE2J1 promoter. HT-29 and HCT 116 showed full methylation (M), DLD-1, LoVo, SW620, SW480, and Caco-2 displayed partial methylation, and NCM460 was unmethylated (U). IVD (in vitro methylated DNA) and NL (normal lymphocyte DNA) served as methylated and unmethylated controls, respectively. **d** BSP validated the methylation profile of UBE2J1 in DLD-1, LoVo, HT-29, and HCT 116 cells. Filled circles represent methylated CpG sites, while open circles indicate unmethylated sites. **e** Representative MSP results in primary CRC tissues (T) and matched adjacent normal tissues (N) demonstrated promoter methylation in the majority of tumor samples but not in the normal counterparts. All quantitative data are presented as mean ± SD from three independent experiments.

UBE2J1 restricts proliferation and metastasis of CRC cells in vitro and in vivo

Expression levels of UBE2J1 were first evaluated in seven CRC cell lines and normal colonic epithelial cells (NCM460) using qRT-PCR and western blotting. DLD-1 and LoVo exhibited relatively higher UBE2J1 expression, whereas HT-29 and HCT 116 showed low expression (**Figures 2a and b**).

To manipulate UBE2J1 levels, DLD-1 and LoVo were transduced with shRNA constructs (sh-UBE2J1#1 and sh-UBE2J1#3, which showed the most effective knockdown), and HT-29 and HCT 116 were engineered to overexpress UBE2J1 via lentiviral infection. Transfection efficiency was verified before proceeding with functional studies (**Figures 2c and d**).

Cell proliferation assays—including CCK-8, colony formation, and EdU incorporation—demonstrated that silencing UBE2J1 enhanced growth, increased colony number and size, and raised the fraction of EdU-positive cells in DLD-1 and LoVo. Conversely, overexpressing UBE2J1 in HT-29 and HCT 116 cells suppressed these parameters (**Figures 3a–f**).

Cell motility and invasive potential were assessed using scratch wound healing and transwell assays. Knockdown of UBE2J1 markedly promoted migration and invasion in DLD-1 and LoVo cells, whereas overexpression reduced these abilities in HT-29 and HCT 116 cells (**Figures**. **3g, h; 4a and b**).

Overall, these findings indicate that UBE2J1 acts as a tumor suppressor by limiting proliferation and metastasis in CRC cells in vitro.

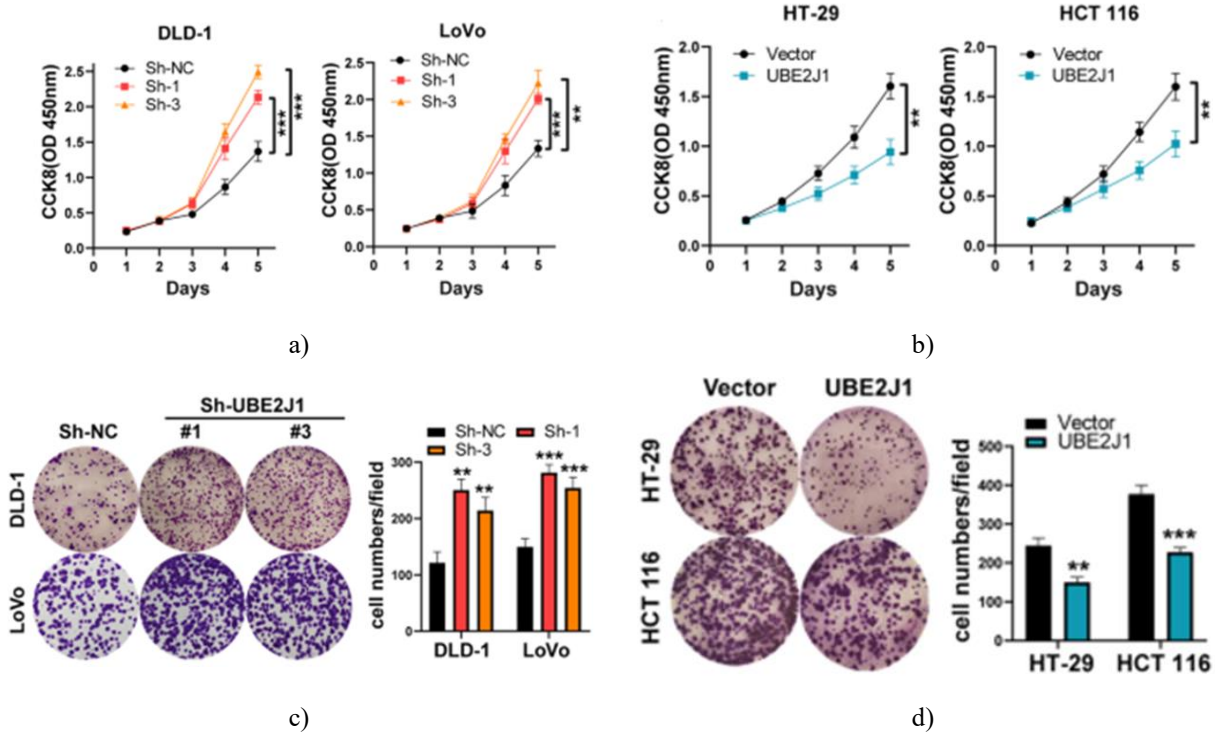

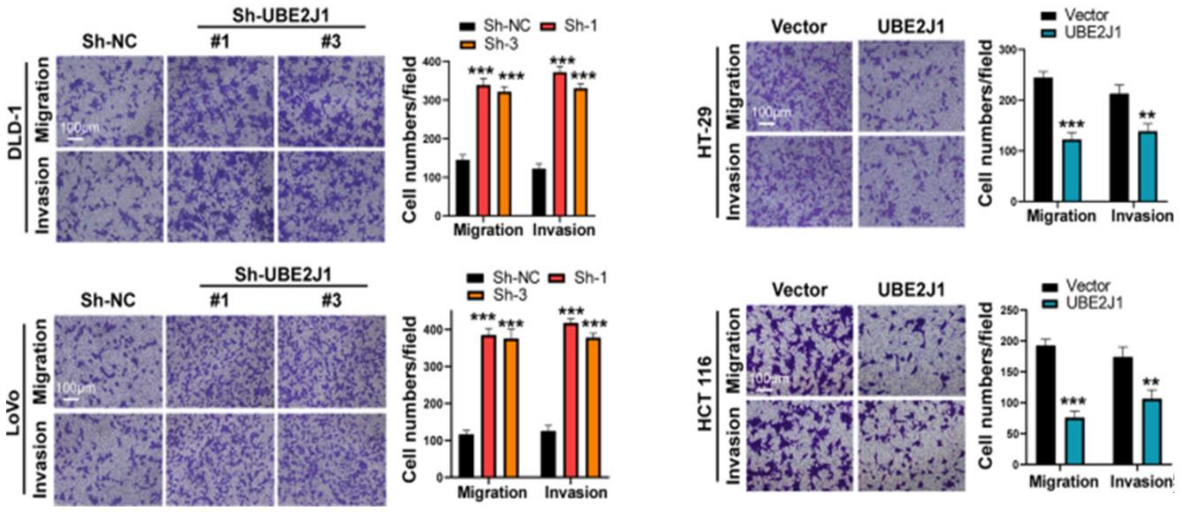

e) f)

Figure 3. UBE2J1 inhibits CRC metastasis and cell proliferation in vitro

a, b The effect of altering UBE2J1 expression on CRC cell viability was examined using CCK-8 assays. Cells with UBE2J1 knockdown showed enhanced proliferation, while UBE2J1-overexpressing cells displayed reduced growth rates. **c, d** Colony formation assays were performed to investigate the long-term proliferative potential. Suppression of UBE2J1 resulted in an increased number and size of colonies, whereas UBE2J1 overexpression limited colony formation. **e, f** EdU incorporation assays were conducted to quantify DNA synthesis as a measure of cell proliferation. Knockdown of UBE2J1 elevated the proportion of EdU-positive cells, whereas overexpression reduced it. **g, h** The migration and invasion capacities of CRC cells were assessed with transwell assays. UBE2J1 depletion significantly promoted both migration and invasion, while overexpression attenuated these abilities.

All results are expressed as mean ± SD from three independent experiments. Statistical significance was indicated as ***P < 0.001, **P < 0.01, *P < 0.05.

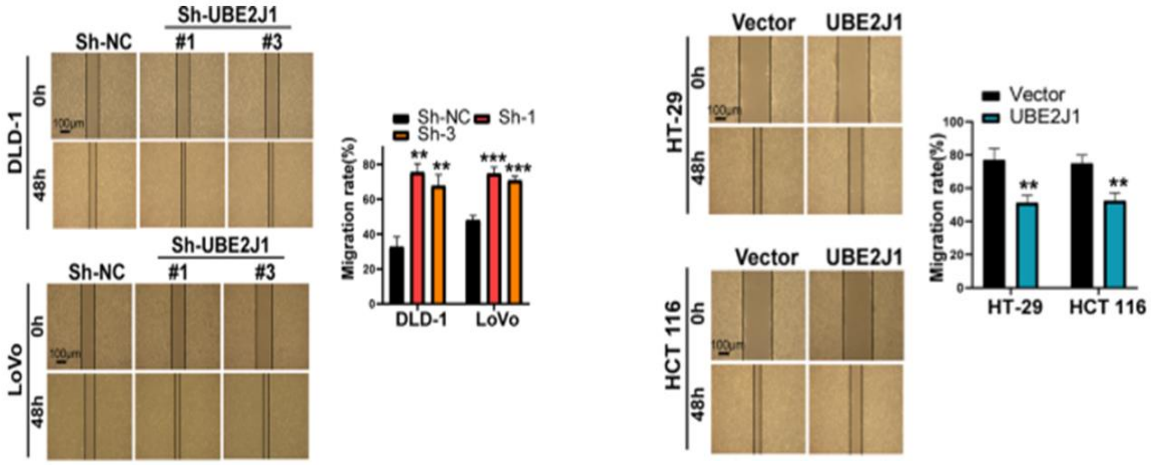

a) b)

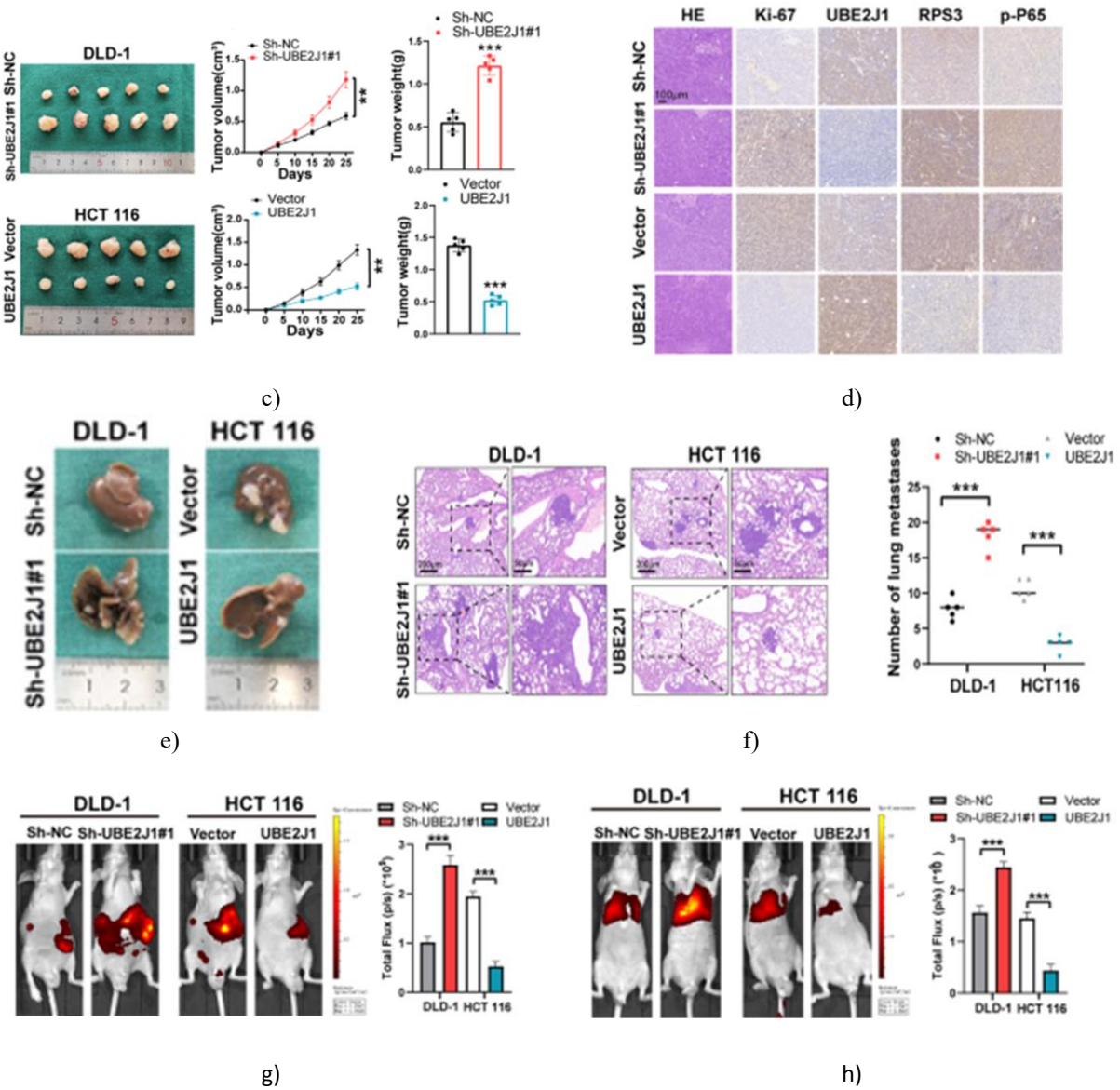

Figure 4: Effects of UBE2J1 on CRC migration, cells proliferation, and invasion in vitro and in vivo

a, b Wound healing assays were conducted to compare the motility of CRC cells with altered UBE2J1 expression. Cells lacking UBE2J1 displayed accelerated closure of the scratch, whereas overexpression slowed migration. **c** Representative images illustrate subcutaneous tumors formed in nude mice. Tumor growth was evaluated by measuring size and calculating average tumor weight. **d** IHC staining was performed to examine protein levels of Ki-67, UBE2J1, RPS3, and phosphorylated P65 (p-P65) in xenograft tumors. **e, g** Representative images depict liver and lung metastases derived from CRC cells in nude mice. **f, h** Histological assessment of metastatic nodules in liver and lung was performed using H&E staining. **i, j** Bioluminescence imaging and quantitative analysis show the intensity of liver and lung metastases.

All experiments were conducted in triplicate and data are shown as mean ± SD. Statistical significance: ***$P < 0.001$, **$P < 0.01$.

To assess the in vivo role of UBE2J1 in tumor growth, DLD-1 and HCT 116 cells were engineered to either knock down or overexpress UBE2J1 using lentiviral transduction. Xenograft experiments demonstrated that tumors derived from UBE2J1-deficient cells grew larger and weighed more than controls. Conversely, tumors

from cells overexpressing UBE2J1 exhibited slower growth and smaller mass (**Figure 4c**).

IHC analysis showed that Ki-67, RPS3, and p-P65 were upregulated in UBE2J1 knockdown tumors, whereas their expression was decreased in UBE2J1-overexpressing tumors, indicating a negative correlation between UBE2J1 and these markers (**Figure 4d**).

To investigate metastatic potential, liver and lung metastasis models were established. Knockdown of UBE2J1 significantly increased both the number of metastatic nodules and bioluminescence signal, while overexpression of UBE2J1 reduced metastatic burden in both organs (**Figures 4e–j**). These results support that UBE2J1 inhibits both proliferation and metastasis of CRC cells in vivo.

UBE2J1 interacts with RPS3 and negatively regulates its protein level

Mass spectrometry combined with immunoprecipitation was employed to identify proteins interacting with UBE2J1. Silver staining revealed multiple unique bands in the UBE2J1 IP group that were absent in IgG controls (**Figure 5a**). Among the top ten candidates, RPS3 was highly abundant aside from structural proteins (**Figures. 5b and 2e**).

IHC analysis of a tissue microarray from cohort 2 indicated that RPS3 levels were elevated in CRC tissues compared to adjacent normal tissues, consistent with TCGA database observations (**Figures 5c, d and 2g**). Kaplan-Meier analysis demonstrated that high RPS3 expression correlated with worse overall survival (**Figure 5e**). Importantly, RPS3 expression was inversely correlated with UBE2J1 levels in CRC tissues (**Figures 5f and g**), highlighting that UBE2J1 may suppress CRC progression through downregulation of RPS3.

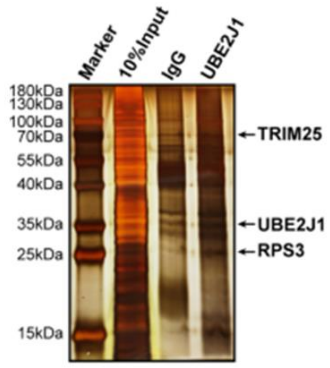

a)

No.	Description	Abundance
1	Ubiquitin-conjugating enzyme E2 J1	117041057.5
2	Keratin, type II cytoskeletal 1	113099245.5
3	40S ribosomal protein S3	99266856.1
4	Keratin, type I cytoskeletal 10	97334523.3
5	Putative elongation factor 1-alpha-like 3	81704157.5
6	E3 ubiquitin/ISG15 ligase TRIM25	78632132.3
7	Keratin, type II cytoskeletal 2 epidermal	71741265.4
8	Eukaryotic translation initiation factor 3 subunit G	56531211.8
9	Heat shock cognate 71 kDa protein	53970289.6
10	Actin, cytoplasmic 1	47255238.7

b)

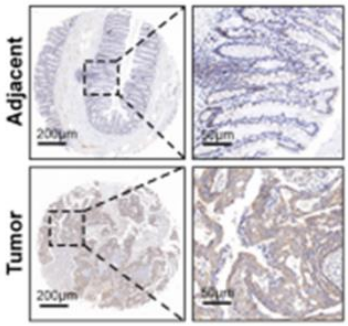

c)

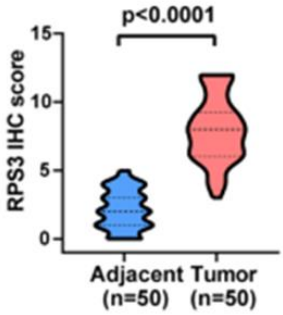

d)

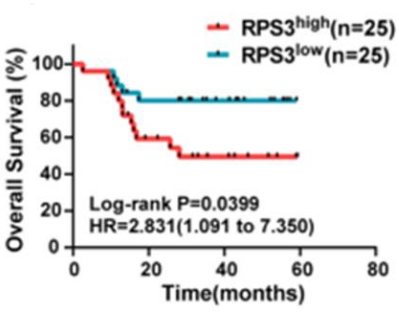

e)

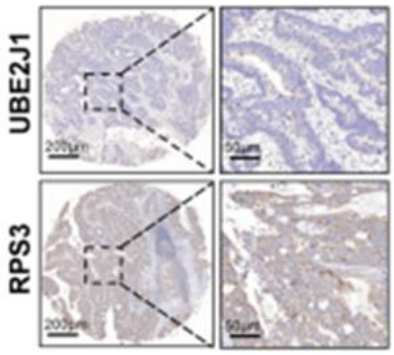
UBE2J1
RPS3

f)

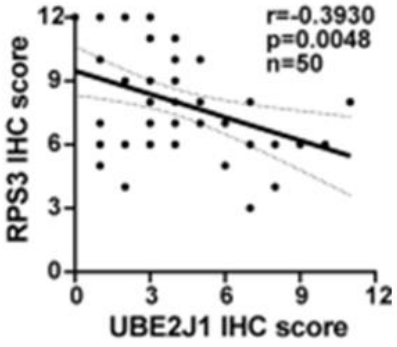
r=-0.3930
p=0.0048
n=50
RPS3 IHC score
UBE2J1 IHC score
0
3
6
9
12

g)

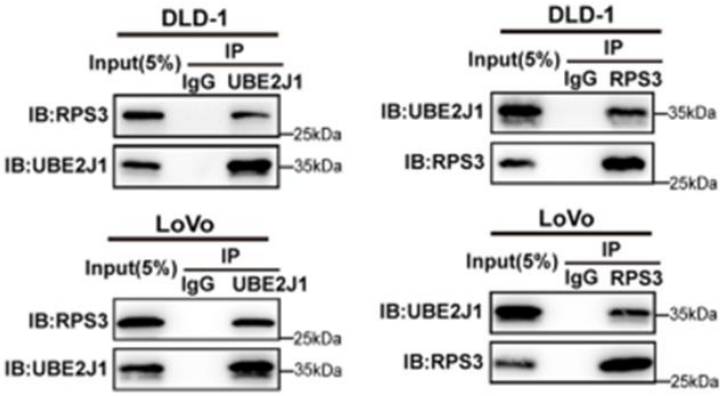
DLD-1
Input(5%)
IP
IgG
UBE2J1
IB:RPS3
IB:UBE2J1
25kDa
35kDa
DLD-1
Input(5%)
IP
IgG
RPS3
IB:UBE2J1
IB:RPS3
35kDa
25kDa
LoVo
Input(5%)
IP
IgG
UBE2J1
IB:RPS3
IB:UBE2J1
25kDa
35kDa
LoVo
Input(5%)
IP
IgG
RPS3
IB:UBE2J1
IB:RPS3
35kDa
25kDa

h)

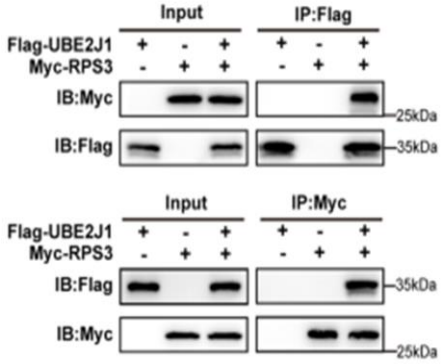
Input
IP:Flag
Flag-UBE2J1
Myc-RPS3
IB:Myc
IB:Flag
25kDa
35kDa
Input
IP:Myc
Flag-UBE2J1
Myc-RPS3
IB:Flag
IB:Myc
35kDa
25kDa

i)

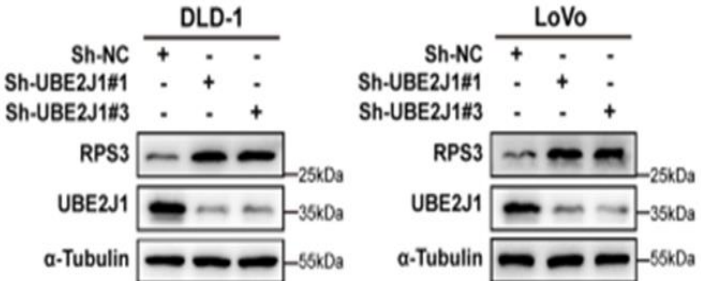
DLD-1
Sh-NC
Sh-UBE2J1#1
Sh-UBE2J1#3
RPS3
UBE2J1
α-Tubulin
25kDa
35kDa
55kDa
LoVo
Sh-NC
Sh-UBE2J1#1
Sh-UBE2J1#3
RPS3
UBE2J1
α-Tubulin
25kDa
35kDa
55kDa

j)

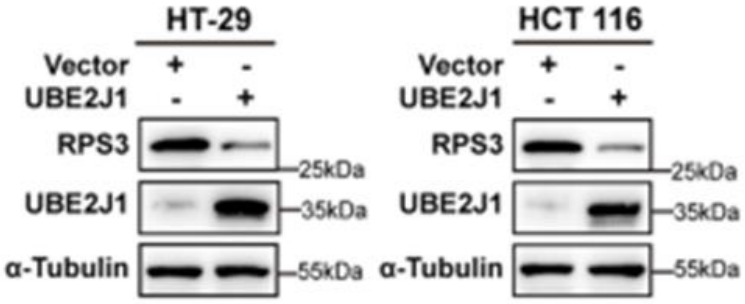
HT-29
Vector
UBE2J1
RPS3
UBE2J1
α-Tubulin
25kDa
35kDa
55kDa
HCT 116
Vector
UBE2J1
RPS3
UBE2J1
α-Tubulin
25kDa
35kDa
55kDa

k)

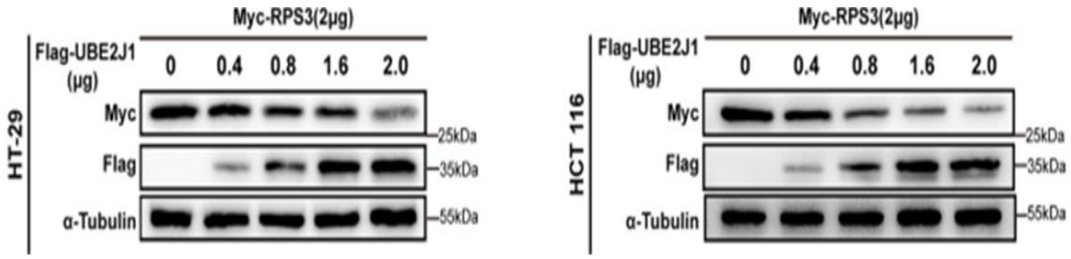

l)

Figure 5. UBE2J1 interacts with RPS3 and negatively regulates its protein level

a Silver staining following UBE2J1 immunoprecipitation in DLD-1 cells revealed distinct protein bands absent in the IgG control. Cells transfected with UBE2J1 lentivirus were separated into input, IgG, and UBE2J1 IP groups for analysis. **b** Mass spectrometry identified the top ten proteins enriched in the UBE2J1 IP fraction. **c–e** IHC evaluation of RPS3 in cohort 2: **c** representative staining images, **d** quantification of IHC scores, **E** Kaplan–Meier curves comparing survival of RPS3^low (n = 25) versus RPS3^high (n = 25) patients. **f, g** Representative IHC images and correlation analysis demonstrating the inverse relationship between UBE2J1 and RPS3 expression in CRC tissues. **h** DLD-1 and LoVo cells were treated with MG132 (10 μM) for 8 hours, followed by co-immunoprecipitation and western blot to examine endogenous UBE2J1-RPS3 binding. **i** HEK293T cells were co-transfected with UBE2J1 and RPS3 plasmids for 24 h, treated with MG132, and interactions were detected via co-IP and western blot. **j, k** Western blotting of CRC cells following UBE2J1 knockdown or overexpression to assess RPS3 protein levels. **l** HT-29 and HCT 116 cells were co-transfected with Myc-RPS3 and increasing amounts of Flag-UBE2J1 for 24 h, then analyzed by western blotting.

All data are presented as mean ± SD of three independent experiments. $P < 0.05$ was considered statistically significant.

Co-immunoprecipitation confirmed that UBE2J1 physically associates with RPS3. Endogenous UBE2J1 co-precipitated with RPS3 and vice versa in DLD-1 and LoVo cells (**Figure 5h**), while exogenously expressed proteins also formed a complex in HEK293T cells (**Figure 5i)**. Given that UBE2J1 is an E2 ubiquitin-conjugating enzyme [12], we hypothesized that RPS3 might be its substrate. Consistent with this, shRNA-mediated knockdown of UBE2J1 increased endogenous RPS3 protein levels (**Figure 5j**), whereas UBE2J1 overexpression decreased RPS3 in a dose-dependent manner (**Figures 5k and 5l**). Notably, RPS3 mRNA levels remained unchanged (**Figure 2h**), indicating post-transcriptional regulation. These results demonstrate that UBE2J1 binds to RPS3 and controls its protein abundance.

Degradation and poly-ubiquitination of RPS3 are promoted by UBE2J1 via targeting K214 residue

To determine whether UBE2J1 regulates RPS3 through ubiquitination, two catalytic mutants of UBE2J1 were generated: M1 (C91S) and M2 (UBC domain deletion), as these regions are critical for its enzymatic activity (**Figure 6a**) [30]. Overexpression of wild-type UBE2J1 promoted RPS3 degradation, whereas both mutants failed to reduce RPS3 levels (**Figure 6b**).

Additionally, WT UBE2J1 enhanced poly-ubiquitination of RPS3 relative to the mutants (**Figure 6c**). The half-life of endogenous RPS3 was shortened by WT UBE2J1, whereas the M1 mutant abrogated this effect (**Figure 6d**). Collectively, these findings confirm that UBE2J1 functions as an E2 enzyme to catalyze RPS3 ubiquitination and degradation.

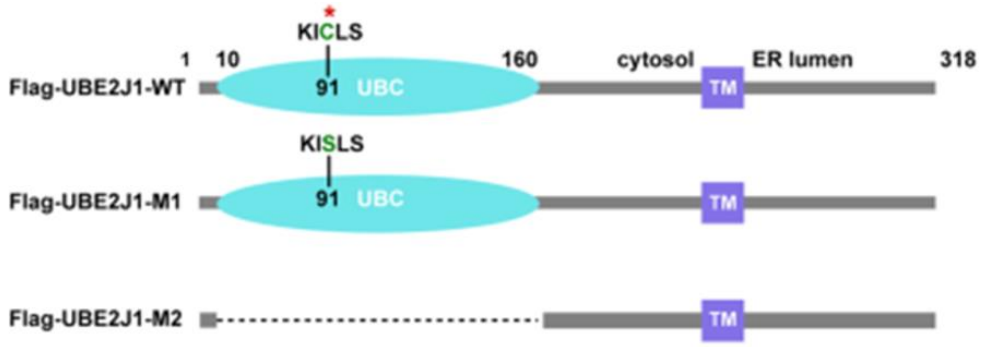
KICLS
1
10
91
UBC
160
cytosol
ER lumen
318
TM
Flag-UBE2J1-WT
KISLS
Flag-UBE2J1-M1
Flag-UBE2J1-M2

a)

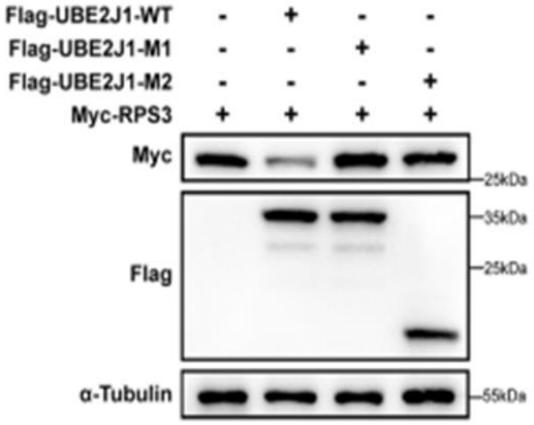
Flag-UBE2J1-WT
Flag-UBE2J1-M1
Flag-UBE2J1-M2
Myc-RPS3
Myc
Flag
α-Tubulin
25kDa
35kDa
55kDa

b)

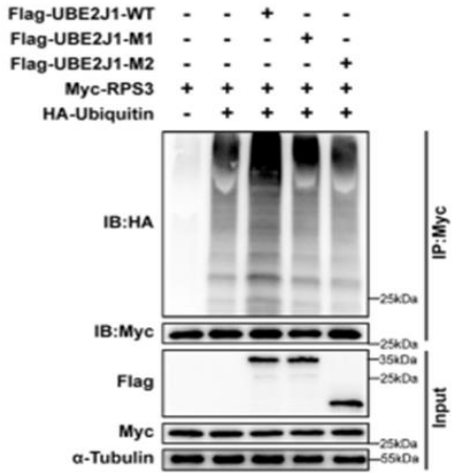
Flag-UBE2J1-WT
Flag-UBE2J1-M1
Flag-UBE2J1-M2
Myc-RPS3
HA-Ubiquitin
IB:HA
IB:Myc
Flag
Myc
α-Tubulin
IP:Myc
Input
25kDa
35kDa
55kDa

c)

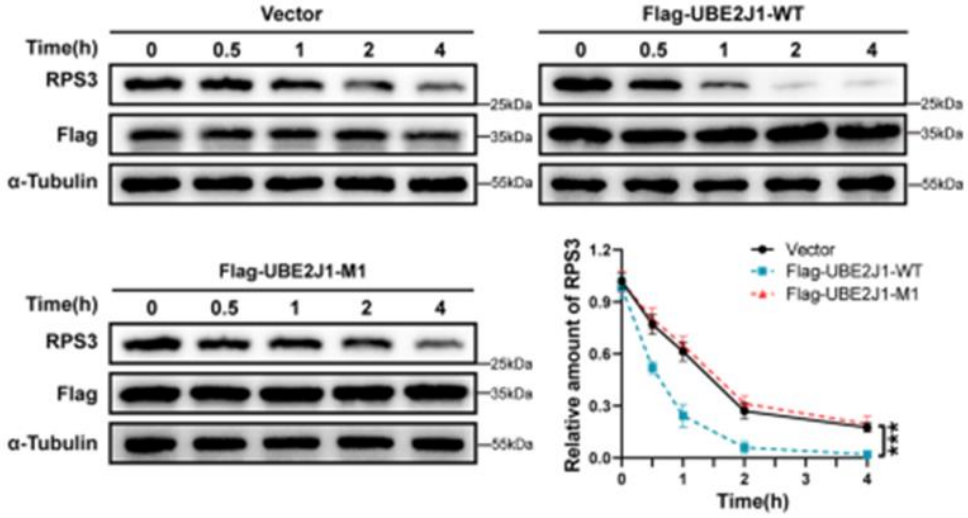
Vector
Flag-UBE2J1-WT
Flag-UBE2J1-M1
Time(h)
0
0.5
1
2
4
RPS3
Flag
α-Tubulin
25kDa
35kDa
55kDa
Relative amount of RPS3
Time(h)
Vector
Flag-UBE2J1-WT
Flag-UBE2J1-M1
***

d)

e)

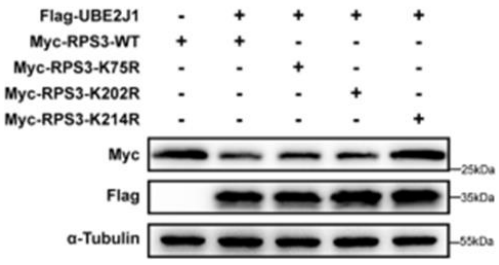

f)

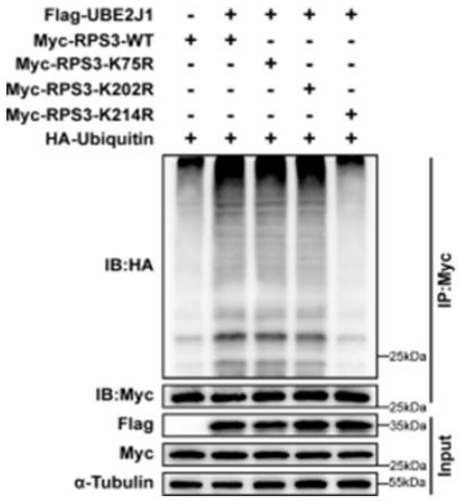

g)

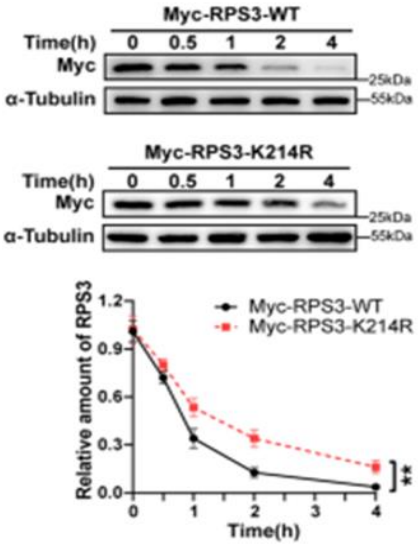

h)

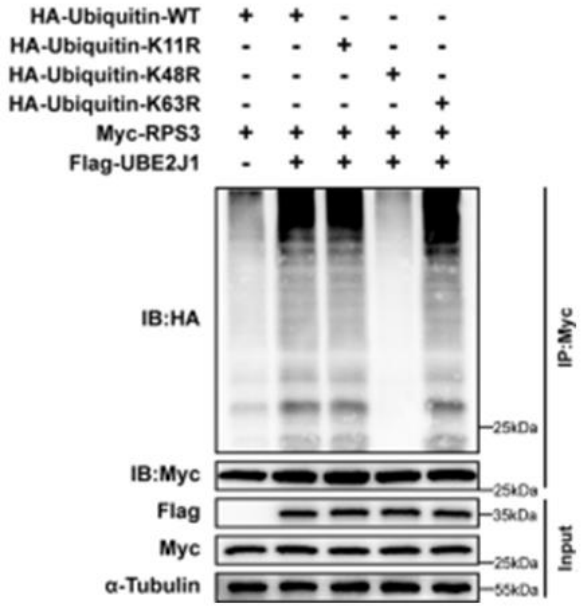

i)

Figure 6. UBE2J1 drives poly-ubiquitination and degradation of RPS3 at the K214 site

a Diagram illustrating wild-type UBE2J1 and the generated mutants. **b** HEK-293T cells were co-transfected with Myc-RPS3 and either Flag-tagged wild-type UBE2J1 or mutants M1/M2. Lysates were collected after 24 h and analyzed via western blot. **c** Cells transfected as indicated were treated with MG132 (10 μM) for 8 h before performing immunoprecipitation with anti-Myc antibodies, followed by western blotting. **d** HEK-293T cells were transfected with vector, Flag-UBE2J1, or the M1 mutant for 24 h, then exposed to CHX (100 μg/mL). Samples were harvested at specific time points to evaluate RPS3 stability. Band intensity was quantified using ImageJ. **e** Conservation of K75, K202, and K214 residues in RPS3 across different species. **f** Wild-type or lysine-mutated RPS3 plasmids were transfected into HEK-293T cells with or without UBE2J1. Protein levels were assessed by western blot after 24 h. **g** Co-IP analysis of poly-ubiquitination of RPS3 in HEK-293T cells transfected with indicated constructs and treated with MG132. **h** Stability assay comparing RPS3-WT and RPS3-K214R following CHX treatment. **i** HEK-293T cells were co-transfected with Flag-UBE2J1, Myc-RPS3, and either wild-type or mutant HA-ubiquitin. After MG132 treatment, co-IP and western blotting were performed.

All results represent mean ± SD of three independent experiments. $^{**}P < 0.01$, $^{***}P < 0.001$.

RPS3, a 40S ribosomal subunit component, is known to undergo ubiquitination controlled by various E3 ligases and deubiquitinases, which regulate ribosome quality control (RQC) [31-34]. To pinpoint the UBE2J1-targeted lysine, we selected conserved residues previously identified as ubiquitination sites [35]. RPS3 mutants (K75R, K202R, K214R) were generated. Overexpression of UBE2J1 triggered degradation of RPS3-WT, K75R, and K202R, but not K214R (**Figure 6f**). Similarly, poly-ubiquitination was blocked in the K214R mutant while remaining unaffected in K75R or K202R (**Figure 6g**). Half-life analysis confirmed that K214R RPS3 was more stable than WT (**Figure 6h**). Further, UBE2J1 selectively induced K48-linked poly-ubiquitination of RPS3, with negligible effect on K11- or K63-linked chains (**Figure 6i**). These findings indicate that K214 is the primary residue mediating UBE2J1-driven RPS3 ubiquitination and proteasomal degradation.

UBE2J1 suppresses NF-κB nuclear translocation by downregulating RPS3

Because RPS3 enhances NF-κB activity [29], we investigated whether UBE2J1 could indirectly inhibit this pathway. Knockdown of UBE2J1 elevated p-P65 levels in whole-cell lysates, increased nuclear P65, and boosted DNA-binding activity, whereas concurrent RPS3 knockdown reversed these effects (**Figures 3a and c**). Conversely, UBE2J1 overexpression reduced p-P65 and nuclear P65 levels and dampened DNA-binding activity; reintroducing RPS3 restored pathway activity (**Figures 3b and d**). Collectively, UBE2J1 suppresses NF-κB signaling by promoting RPS3 degradation.

TRIM25 collaborates with UBE2J1 to enhance RPS3 ubiquitination

Since E2 enzymes rely on E3 ligases to target substrates [7, 8], we analyzed mass spectrometry data for potential partners. TRIM25, a RING-type E3 ligase, was identified as a prominent UBE2J1-interacting protein (**Figure**s. **5b and 2f**). Reciprocal co-IP confirmed binding between TRIM25 and UBE2J1 (**Figures 7a and b**). Co-expression of TRIM25 and UBE2J1 markedly enhanced RPS3 degradation and poly-ubiquitination relative to single expression (**Figures 7c and e**), whereas TRIM25 knockdown attenuated these effects (**Figures 7d and f**). Domain mapping showed that the RING domain of TRIM25 interacts with the UBC domain of UBE2J1, while the PRY/SPRY domain of TRIM25 binds the C-terminal region of RPS3 (**Figures 3e–j and g–j**). Functional assays revealed that dual knockdown of TRIM25 and UBE2J1 further increased nuclear p-P65 and DNA-binding activity compared with UBE2J1 depletion alone, but these effects were reversed by RPS3 knockdown (**Figures 7g and 7i**). Conversely, co-overexpression suppressed NF-κB activity more strongly than either alone (**Figures 7h and 7j**). These data indicate that UBE2J1 forms an E2-E3 complex with TRIM25 to ubiquitinate and degrade RPS3, thereby inhibiting NF-κB signaling in CRC.

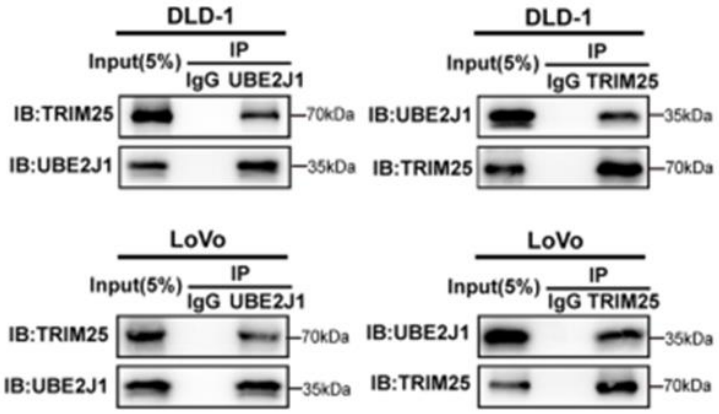
DLD-1
Input(5%)
IP
IgG UBE2J1
IB:TRIM25
70kDa
IB:UBE2J1
35kDa
DLD-1
Input(5%)
IP
IgG TRIM25
IB:UBE2J1
35kDa
IB:TRIM25
70kDa
LoVo
Input(5%)
IP
IgG UBE2J1
IB:TRIM25
70kDa
IB:UBE2J1
35kDa
LoVo
Input(5%)
IP
IgG TRIM25
IB:UBE2J1
35kDa
IB:TRIM25
70kDa

a)

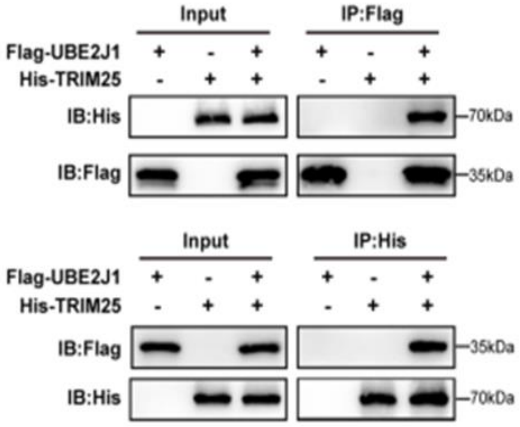
Input
IP:Flag
Flag-UBE2J1 + - + + - +
His-TRIM25 - + + - + +
IB:His
70kDa
IB:Flag
35kDa
Input
IP:His
Flag-UBE2J1 + - + + - +
His-TRIM25 - + + - + +
IB:Flag
35kDa
IB:His
70kDa

b)

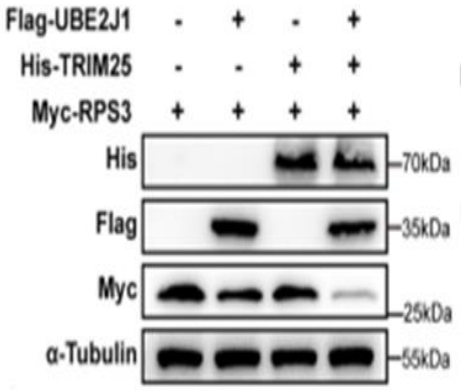
Flag-UBE2J1 - + - +
His-TRIM25 - - + +
Myc-RPS3 + + + +
His
70kDa
Flag
35kDa
Myc
25kDa
α-Tubulin
55kDa

c)

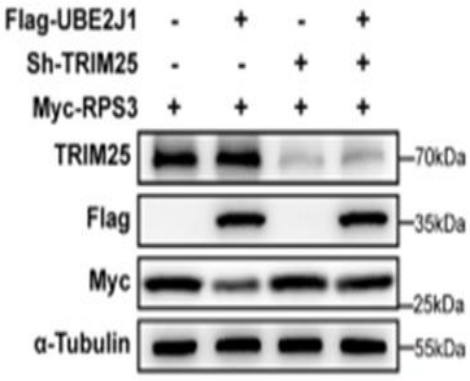
Flag-UBE2J1 - + - +
Sh-TRIM25 - - + +
Myc-RPS3 + + + +
TRIM25
70kDa
Flag
35kDa
Myc
25kDa
α-Tubulin
55kDa

d)

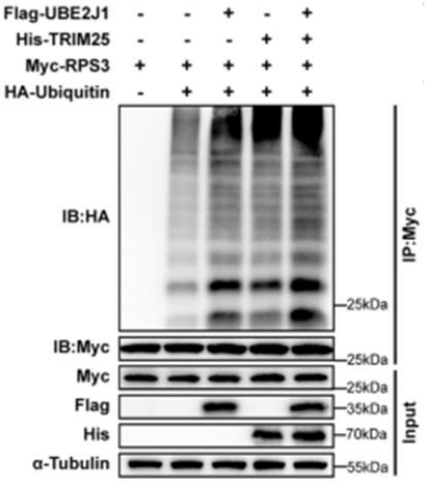
Flag-UBE2J1 - - + - +
His-TRIM25 - - - + +
Myc-RPS3 + + + + +
HA-Ubiquitin - + + + +
IB:HA
25kDa
IP:Myc
IB:Myc
25kDa
Myc
25kDa
Flag
35kDa
His
70kDa
α-Tubulin
55kDa
Input

e)

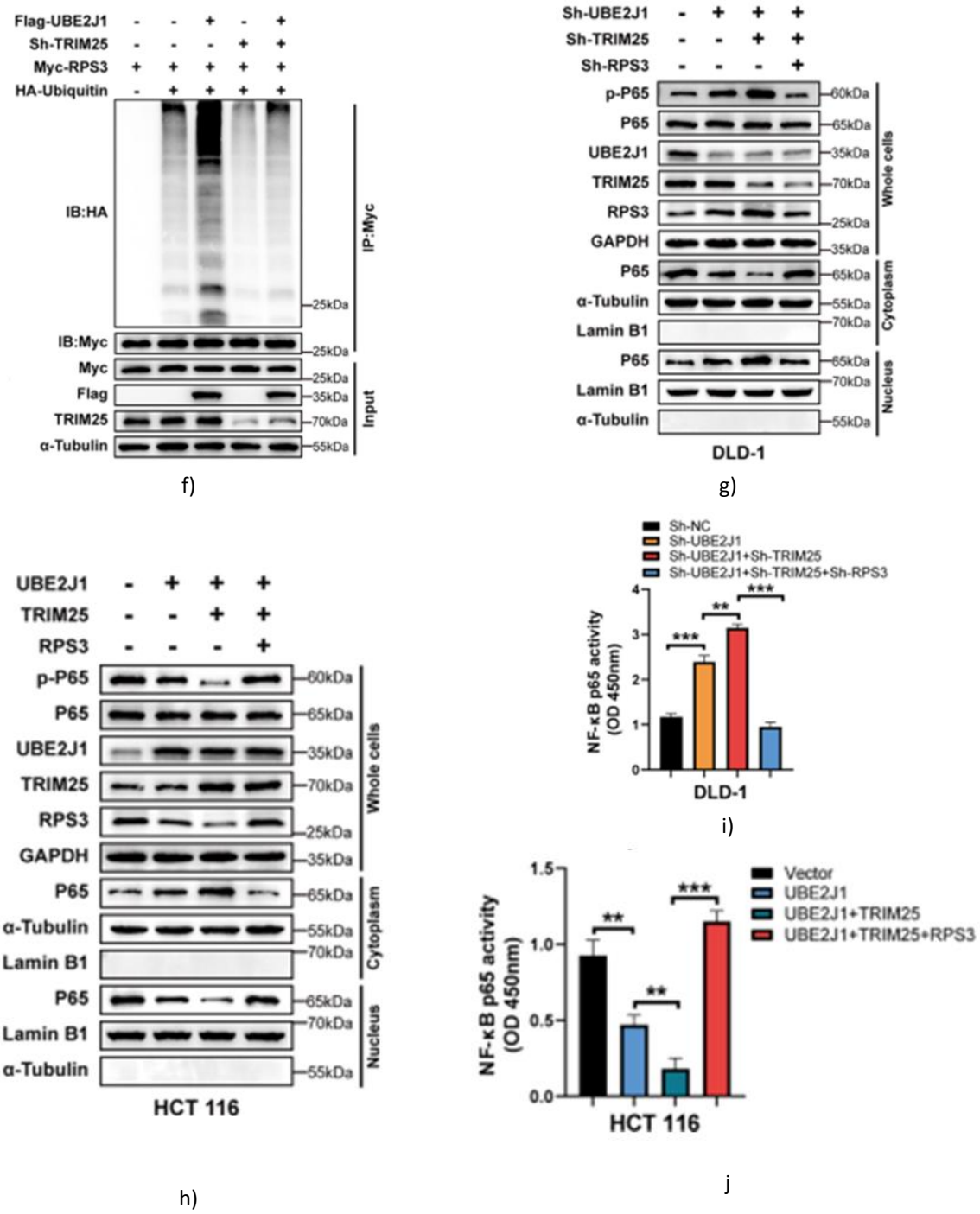

Figure 7. TRIM25 synergizes with UBE2J1 to drive RPS3 poly-ubiquitination and degradation, suppressing NF-κB signaling

a The interaction between endogenous UBE2J1 and TRIM25 in DLD-1 and LoVo cells was validated using co-immunoprecipitation (co-IP) followed by western blotting. **b** HEK-293T cells transfected with the indicated plasmids for 24 h demonstrated exogenous binding between UBE2J1 and TRIM25, as shown by co-IP and western blotting. **c, d** Western blot analyses assessed the combined effects of TRIM25 and UBE2J1 on RPS3 protein abundance. **e, f** To evaluate RPS3 ubiquitination, HEK-293T cells expressing the indicated plasmids were treated with MG132 (10 μM) for 8 h. Lysates were immunoprecipitated with anti-Myc antibodies and

probed for ubiquitination by western blotting. **g, h** The levels of p-P65 and P65 were examined in total, nuclear, and cytoplasmic fractions from HCT 116 and DLD-1 cells stably expressing indicated lentiviruses. GAPDH, α-Tubulin, and Lamin B1 served as loading controls. **i, j** Nuclear extracts from DLD-1 and HCT 116 cells were analyzed for P65 DNA-binding activity.

All data are represented as mean ± SD of three independent experiments. ***P < 0.001, **P < 0.01.

UBE2J1 restrains CRC cell growth and metastasis via RPS3 inhibition

To clarify whether RPS3 mediates the tumor-suppressive role of UBE2J1, we performed functional rescue experiments. CRC cells with stable UBE2J1 knockdown or controls were transduced with lentiviruses encoding either shRNA-RPS3 or a non-targeting control. Meanwhile, UBE2J1-overexpressing cells were co-infected with lentiviruses expressing RPS3 or vector controls. Suppression of RPS3 in UBE2J1-deficient cells counteracted the accelerated cell proliferation observed in CCK-8 assays **(Figure 4a),** whereas ectopic RPS3 expression restored proliferation in cells with UBE2J1 overexpression **(Figure 4b).**

Similar results were observed in colony formation and EdU assays: RPS3 knockdown in UBE2J1-depleted cells rescued colony numbers and DNA replication activity, and RPS3 overexpression mitigated the proliferation inhibition in UBE2J1-overexpressing cells (**Figures 4c–f).**

Functional migration and invasion studies using transwell and wound healing assays showed that RPS3 depletion reversed the increased motility and invasiveness of UBE2J1 knockdown cells, whereas RPS3 overexpression partially restored migration and invasion in cells overexpressing UBE2J1 (**Figures 5a, 5b, 6a and 6b**).

Together, these findings confirm that UBE2J1 exerts its inhibitory effects on CRC cell proliferation and metastasis predominantly through downregulation of RPS3.

UBE2J1, a member of the E2 ubiquitin-conjugating enzyme family, has been widely recognized for its role in mediating the ubiquitination and degradation of ER-associated degradation (ERAD) substrates [13-15]. Despite this, few studies have explored its function in cancer development. Previous reports indicate that elevated UBE2J1 levels correlate with poor prognosis in prostate cancer [18], and more recently, UBE2J1 has been implicated in medulloblastoma progression and in promoting endometrial cancer [17, 19]. In the present study, we provide the first evidence that UBE2J1 functions as a tumor suppressor in colorectal cancer (CRC), inhibiting both cell proliferation and metastatic potential through an RPS3-dependent mechanism. Clinically, UBE2J1 expression was significantly reduced in CRC patient samples, and lower levels were associated with adverse clinicopathological features and poor prognosis, suggesting its potential as a predictive biomarker for CRC diagnosis and patient outcomes.

RPS3 has been reported to be upregulated in colorectal tumors and adenomas compared to normal colonic epithelium [36]. Functional studies have shown that RPS3 depletion decreases proliferation, survival, migration, and invasion, while promoting apoptosis in CRC cell lines such as Caco-2 [37], consistent with our observations. In our cohort and the TCGA dataset, RPS3 was elevated in CRC tissues, and patients with higher RPS3 expression had poorer overall survival. Importantly, RPS3 protein levels negatively correlated with UBE2J1 expression in CRC samples, suggesting that UBE2J1 may act as an upstream regulator of RPS3.

Previous research has demonstrated that RPS3 is a target of ubiquitin-mediated degradation in various contexts. For instance, RNF138 promotes RPS3 degradation to confer radioresistance in glioblastoma cells [38], while the HSP70/CHIP complex mediates ubiquitination and proteasomal degradation of RPS3 [39], a process that can be inhibited by HSP90 through direct binding [40]. Additionally, circPLCE1 411 has been reported to interact with the HSP90α/RPS3 complex, promoting RPS3 degradation and thereby suppressing NF-κB activity in CRC [41]. Extending these findings, our proteomic analysis identified UBE2J1 as a novel upstream regulator of RPS3, facilitating its ubiquitin-dependent proteasomal degradation in a post-transcriptional manner. Mass spectrometry further revealed TRIM25 as a potential E3 ligase partner, and subsequent experiments confirmed that UBE2J1 and TRIM25 cooperate to decrease RPS3 protein levels and enhance its poly-ubiquitination.

Aberrant activation of the NF-κB pathway is widely recognized to contribute to CRC progression, affecting proliferation, migration, and metastasis [42-44]. Elevated nuclear p65 accumulation has been associated with advanced disease stage and worse prognosis [45, 46], highlighting the clinical relevance of NF-κB inhibition. Several clinical trials are currently evaluating NF-κB

inhibitors for CRC therapy [47, 48]. In our study, we demonstrated that UBE2J1 impairs NF-κB signaling by preventing p65 nuclear translocation in an RPS3-dependent manner. Rescue experiments showed that RPS3 overexpression restored nuclear p65 accumulation and DNA-binding activity suppressed by UBE2J1, while functional assays confirmed that UBE2J1 inhibits CRC cell proliferation and metastasis through RPS3 downregulation. Collectively, these findings reveal a novel UBE2J1/TRIM25–RPS3–NF-κB axis that governs CRC progression and may represent a promising therapeutic target for intervention (**Figure 8**).

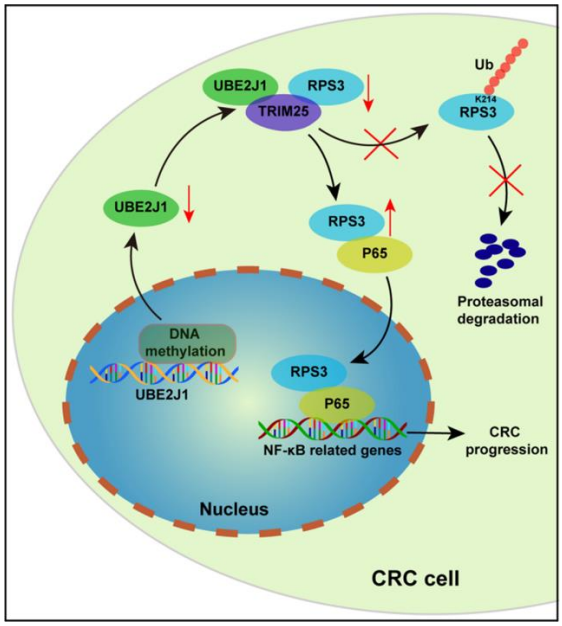

Figure 8. Mechanistic overview of UBE2J1 in CRC

In brief, our study reveals that UBE2J1 functions as a tumor suppressor in colorectal cancer, and its expression is suppressed through promoter hypermethylation. Mechanistically, UBE2J1 collaborates with TRIM25 to specifically target RPS3 at the K214 site, promoting its poly-ubiquitination and subsequent degradation, which in turn inhibits the activation of the NF-κB signaling cascade.

Materials and Methods

Human tissue samples and ethical considerations

Colorectal cancer specimens were collected from patients at the General Surgery Department of the First Affiliated Hospital of Nanjing Medical University, following signed informed consent. Immediately after surgical excision, tissues were snap-frozen and stored at −80 °C. Importantly, none of the enrolled patients had received preoperative chemotherapy or radiotherapy.

Cell culture

The following human cell lines were used in this study: LoVo, DLD-1, SW480, SW620, HT-29, Caco-2, NCM460, HCT 116, and HEK-293T. All cell lines were obtained from the Cell Bank of Type Culture Collection of the Chinese Academy of Sciences (Shanghai, China). Cells were cultured in a humidified incubator at 37 °C under an atmosphere containing 5% CO_2.

Quantitative real-time PCR (qRT-PCR)

Total RNA was extracted using TRIzol reagent (Invitrogen, USA) following the manufacturer's instructions. The RNA was then reverse-transcribed into cDNA using the HiScript RT Mix kit (Vazyme, Jiangsu, China). Quantitative PCR amplification was performed using the SYBR Premix Ex Taq Kit (TaKaRa Biotechnology, Dalian, China). StepOne software v2.3 was used for data acquisition and analysis.

Cell transfection

shRNA sequences targeting RPS3 and UBE2J1 were packaged into lentiviral vectors by Obio (Shanghai, China). Full-length UBE2J1 and RPS3 cDNAs were cloned into lentiviral expression plasmids by Obio. shRNAs for TRIM25 and corresponding negative controls (sh-NC) were obtained from RiboBio (Guangzhou, China), and overexpression plasmids for TRIM25 and ubiquitin were also sourced from Obio. In addition, mutant constructs for RPS3, UBE2J1, and ubiquitin were synthesized by Obio. Transfections of plasmids and shRNAs were performed using Lipofectamine 3000 (Invitrogen, USA), and the efficiency of gene manipulation was verified through qRT-PCR and western blot analysis.

Cell proliferation assays

Cell growth was assessed using the CCK-8 assay (Beyotime, Shanghai, China), colony formation assays, and EdU incorporation assays (Beyotime, Shanghai, China) according to established methods [49]. For quantitative evaluation, the average number of proliferating cells in three randomly selected microscopic fields was calculated for each sample.

Migration and invasion assays

Invasion capabilities and cell migration were measured using Transwell chambers and wound healing (scratch) assays, following previously reported protocols [50]. For each experiment, three independent fields were selected at random for analysis.

Immunohistochemistry (IHC)

IHC was conducted based on previously described procedures [49]. The expression of UBE2J1 and RPS3 was evaluated by combining staining intensity (0–3: 0 = negative, 1 = weak, 2 = moderate, 3 = strong) and the proportion of positively stained cells (0–4: 0 = 0%, 1 = 1–24%, 2 = 25–49%, 3 = 50–74%, 4 = 75–100%). Final IHC scores were determined by multiplying intensity by positivity, and based on the median value, tissues were classified as high or low expression.

Cytoplasmic proteins and extraction of nuclear

Nuclear and cytoplasmic fractions from and HCT 116 and DLD-1 cells were separated using the PARIS™ kit (AM1556, Thermo Fisher Scientific) following the manufacturer's instructions. Proteins from each fraction were collected for western blotting. GAPDH, α-Tubulin, and Lamin B1 were used as loading controls for cytoplasmic and nuclear proteins, respectively.

Antibodies and western blot analysis

Western blotting was performed following the established method outlined previously [51].

Co-immunoprecipitation (Co-IP) assay

To investigate potential direct binding between UBE2J1, RPS3, and TRIM25, experiments were carried out using the Pierce Co-Immunoprecipitation Kit (#88804, Thermo Fisher Scientific). Lysates from cells were combined with the relevant primary antibody and rotated overnight at 4 °C. Protein complexes were then captured by adding A/G magnetic beads and incubating for 1 h at room temperature. Beads underwent two washes in IP lysis buffer followed by a single rinse in ultrapure water. Elution was achieved by resuspending in 1 × SDS sample buffer and heating at 95 °C for 10 min. The resulting immunoprecipitates were resolved by SDS-PAGE for Western blot detection or forwarded for mass spectrometric analysis (performed by BGI Shenzhen, Guangdong, China).

In vivo ubiquitination assay

Following transfection with the designated plasmids or shRNAs, cells were exposed to the proteasomal inhibitor MG132 (Beyotime, Shanghai, China) at a suitable concentration for 8 h to accumulate ubiquitinated species prior to lysis. Lysates underwent immunoprecipitation with anti-Myc antibody to isolate the target complex. Subsequent immunoblotting with anti-HA antibody was used to visualize HA-tagged ubiquitin conjugates on RPS3.

5-Aza-2'-deoxycytidine (5-Aza) treatment

Colorectal cancer (CRC) cell lines were plated at approximately 30% density and allowed to attach for 12 h. Cells were then cultured in medium containing 2 μM 5-aza-2'-deoxycytidine (5-Aza; Sigma, MO, USA), with the compound refreshed daily over a 4-day period. At the conclusion of treatment, cells were harvested, and total RNA was isolated using the previously described procedure.

Bisulfite Sequencing PCR (BSP) and Methylation-specific PCR (MSP)

Genomic DNA from colorectal cancer (CRC) cell lines was isolated using the DNeasy Blood & Tissue Kit (Qiagen). Subsequently, 2 μg of purified genomic DNA was subjected to bisulfite conversion by incubation in bisulfite DNA lysis buffer for 1 h at 37 °C, followed by denaturation and deamination steps. The converted DNA was amplified using methylation-specific PCR (MSP) primers, and the resulting amplicons were separated and visualized on agarose gels via electrophoresis. For bisulfite sequencing PCR (BSP), the treated DNA was similarly amplified with BSP-specific primers. Amplicons were purified, ligated into the pMD19-T vector (TaKaRa, Dalian, China), and transformed for clonal propagation prior to Sanger sequencing.

Animal models

Male BALB/c nude mice aged five weeks were employed to establish subcutaneous xenograft tumors as well as models of liver and lung metastasis. In the subcutaneous xenograft experiments, 1×10^6 DLD-1 cells with stable UBE2J1 knockdown or HCT 116 cells with stable UBE2J1 overexpression—along with their respective control cells—were injected into the left and right flanks of each mouse. Tumor growth was monitored by measuring volume and weight every 5 days. Twenty-five days post-injection, animals were euthanized, and excised tumors were processed for hematoxylin and

eosin (H&E) staining and immunohistochemical (IHC) analysis. For metastasis studies, 1×10^6 luciferase-expressing versions of the aforementioned cells were administered either intrasplenically (for liver metastasis) or via tail vein injection (for lung metastasis). Four weeks later, bioluminescence imaging was performed 10 min after intraperitoneal administration of 150 mg/kg D-luciferin (Goldbio, USA) using the IVIS 100 Imaging System (Xenogen, Hopkinton, MA, USA). Following imaging, mice were euthanized, and liver and lung tissues were harvested for gross examination and H&E staining. All procedures involving animals were conducted in accordance with protocols approved by the Ethics Committee on Animal Experiments at Nanjing Medical University.

Statistical analysis

Data analysis was performed using GraphPad Prism version 9.0 (La Jolla, CA, USA) and SPSS version 13.0 (Chicago, IL, USA). Comparisons were made using Student's t-test, one-way ANOVA, Chi-square test, or Kaplan-Meier survival analysis as appropriate. All experiments were independently replicated at least three times. Results are presented as mean ± standard deviation (SD), with statistical significance defined as $P < 0.05$.

Acknowledgments: We appreciate Dr. Peng Yang for providing technical assistance. We would like to thank the Core Facility of Jiangsu Provincial People's Hospital for its help in the detection of experimental samples. This study was funded by the Primary Research & Development Plan of Jiangsu Province (BE2021742), Jiangsu Provincial Natural Science Foundation for Basic Research, China (Grant No. BK20201491), the National Key R&D Program of China (2017YFC0908200), Jiangsu Key Medical Discipline (General Surgery; Grant No. ZDxKA2016005).

Conflict of Interest: None

Financial Support: None

Ethics Statement: None

References

1. Siegel RL, Miller KD, Fuchs HE, Jemal A. Cancer statistics, 2022. CA Cancer J Clin. 2022;72:7–33.
2. Siegel RL, Miller KD, Jemal A. Cancer statistics, 2020. CA Cancer J Clin. 2020;70:7–30.
3. Dekker E, Tanis PJ, Vleugels JLA, Kasi PM, Wallace MB. Colorectal cancer. Lancet. 2019;394:1467–80.
4. Cassidy S, Syed BA. Colorectal cancer drugs market. Nat Rev Drug Disco. 2017;16:525–6.
5. Swatek KN, Komander D. Ubiquitin modifications. Cell Res. 2016;26:399–422.
6. Senft D, Qi J, Ronai ZA. Ubiquitin ligases in oncogenic transformation and cancer therapy. Nat Rev Cancer. 2018;18:69–88.
7. Rape M. Ubiquitylation at the crossroads of development and disease. Nat Rev Mol Cell Biol. 2018;19:59–70.
8. Song L, Luo ZQ. Post-translational regulation of ubiquitin signaling. J Cell Biol. 2019;218:1776–86.
9. Bui QT, Hong JH, Kwak M, Lee JY, Lee PC. Ubiquitin-conjugating enzymes in cancer. Cells. 2021;10:1383.
10. Popovic D, Vucic D, Dikic I. Ubiquitination in disease pathogenesis and treatment. Nat Med. 2014;20:1242–53.
11. Oh E, Akopian D, Rape M. Principles of ubiquitin-dependent signaling. Annu Rev Cell Dev Biol. 2018;34:137–62.
12. Lester D, Farquharson C, Russell G, Houston B. Identification of a family of noncanonical ubiquitin-conjugating enzymes structurally related to yeast UBC6. Biochem Biophys Res Commun. 2000;269:474–80.
13. Wu CJ, Conze DB, Li X, Ying SX, Hanover JA, Ashwell JD. TNF-alpha induced c-IAP1/TRAF2 complex translocation to a Ubc6-containing compartment and TRAF2 ubiquitination. EMBO J. 2005;24:1886–98.
14. Burr ML, Cano F, Svobodova S, Boyle LH, Boname JM, Lehner PJ. HRD1 and UBE2J1 target misfolded MHC class I heavy chains for endoplasmic reticulum-associated degradation. Proc Natl Acad Sci USA. 2011;108:2034–9.
15. Younger JM, Chen L, Ren HY, Rosser MF, Turnbull EL, Fan CY, et al. Sequential quality-control checkpoints triage misfolded cystic fibrosis transmembrane conductance regulator. Cell. 2006;126:571–82.
16. Feng T, Deng L, Lu X, Pan W, Wu Q, Dai J. Ubiquitin-conjugating enzyme UBE2J1 negatively

modulates interferon pathway and promotes RNA virus infection. Virol J. 2018;15:132.
17. Palmer CJ, Galan-Caridad JM, Weisberg SP, Lei L, Esquilin JM, Croft GF, et al. Zfx facilitates tumorigenesis caused by activation of the Hedgehog pathway. Cancer Res. 2014;74:5914–24.
18. Chen Z, Hu H. Identification of prognosis biomarkers of prostatic cancer in a cohort of 498 patients from TCGA. Curr Probl Cancer. 2019;43:100503.
19. Yang D, Ma X, Xu J, Jia K, Liu X, Zhang P. Zfx-induced upregulation of UBE2J1 facilitates endometrial cancer progression via PI3K/AKT pathway. Cancer Biol Ther. 2021;22:238–47.
20. Hayden MS, Ghosh S. Shared principles in NF-kappaB signaling. Cell. 2008;132:344–62.
21. Baldwin AS Jr. The NF-kappa B and I kappa B proteins: new discoveries and insights. Annu Rev Immunol. 1996;14:649–83.
22. Perkins ND. The diverse and complex roles of NF-kappaB subunits in cancer. Nat Rev Cancer. 2012;12:121–32.
23. Karin M. Nuclear factor-kappaB in cancer development and progression. Nature. 2006;441:431–6.
24. Schafer T, Maco B, Petfalski E, Tollervey D, Bottcher B, Aebi U, et al. Hrr25-dependent phosphorylation state regulates organization of the pre-40S subunit. Nature. 2006;441:651–5.
25. Jang C-Y, Lee JY, Kim J. RpS3, a DNA repair endonuclease and ribosomal protein, is involved in apoptosis. FEBS Lett. 2004;560:81–5.
26. Yang HJ, Youn H, Seong KM, Jin YW, Kim J, Youn B. Phosphorylation of ribosomal protein S3 and antiapoptotic TRAF2 protein mediates radioresistance in non-small cell lung cancer cells. J Biol Chem. 2013;288:2965–75.
27. Graifer D, Malygin A, Zharkov DO, Karpova G. Eukaryotic ribosomal protein S3: A constituent of translational machinery and an extraribosomal player in various cellular processes. Biochimie. 2014;99:8–18.
28. Youn H, Son B, Kim W, Jun SY, Lee JS, Lee JM, et al. Dissociation of MIF-rpS3 complex and sequential NF-kappaB activation is involved in IR-induced metastatic conversion of NSCLC. J Cell Biochem. 2015;116:2504–16.
29. Wan F, Anderson DE, Barnitz RA, Snow A, Bidere N, Zheng L, et al. Ribosomal protein S3: a KH domain subunit in NF-kappaB complexes that mediates selective gene regulation. Cell. 2007;131:927–39.
30. Cremer T, Jongsma MLM, Trulsson F, Vertegaal ACO, Neefjes J, Berlin I. The ER-embedded UBE2J1/RNF26 ubiquitylation complex exerts spatiotemporal control over the endolysosomal pathway. Cell Rep. 2021;34:108659.
31. Meyer C, Garzia A, Morozov P, Molina H, Tuschl T. The G3BP1-family-USP10 deubiquitinase complex rescues ubiquitinated 40S subunits of ribosomes stalled in translation from lysosomal degradation. Mol Cell. 2020;77:1193–1205.e1195.
32. Garzia A, Meyer C, Tuschl T. The E3 ubiquitin ligase RNF10 modifies 40S ribosomal subunits of ribosomes compromised in translation. Cell Rep. 2021;36:109468.
33. Jung Y, Kim HD, Yang HW, Kim HJ, Jang CY, Kim J. Modulating cellular balance of Rps3 mono-ubiquitination by both Hel2 E3 ligase and Ubp3 deubiquitinase regulates protein quality control. Exp Mol Med. 2017;49:e390.
34. Sundaramoorthy E, Leonard M, Mak R, Liao J, Fulzele A, Bennett EJ. ZNF598 and RACK1 regulate mammalian ribosome-associated quality control function by mediating regulatory 40S ribosomal ubiquitylation. Mol Cell. 2017;65:751–760.e754.
35. Higgins R, Gendron JM, Rising L, Mak R, Webb K, Kaiser SE, et al. The unfolded protein response triggers site-specific regulatory ubiquitylation of 40s ribosomal proteins. Mol Cell. 2015;59:35–49.
36. Pogue-Geile K, Geiser JR, Shu M, Miller C, Wool IG, Meisler AI, et al. Ribosomal protein genes are overexpressed in colorectal cancer: isolation of a cDNA clone encoding the human S3 ribosomal protein. Mol Cell Biol. 1991;11:3842–9.
37. Alam E, Maaliki L, Nasr Z. Ribosomal protein S3 selectively affects colon cancer growth by modulating the levels of p53 and lactate dehydrogenase. Mol Biol Rep. 2020;47:6083–90.
38. Kim W, Youn H, Lee S, Kim E, Kim D, Sub Lee J, et al. RNF138-mediated ubiquitination of rpS3 is required for resistance of glioblastoma cells to radiation-induced apoptosis. Exp Mol Med. 2018;50:e434.
39. Hwang I, Cho SW, Ahn JY. Chaperone-E3 ligase complex HSP70-CHIP mediates ubiquitination of ribosomal protein S3. Int J Mol Sci. 2018;19:2723.

40. Kim TS, Jang CY, Kim HD, Lee JY, Ahn BY, Kim J. Interaction of Hsp90 with ribosomal proteins protects from ubiquitination and proteasome-dependent degradation. Mol Biol Cell. 2006;17:824–33.
41. Liang ZX, Liu HS, Xiong L, Yang X, Wang FW, Zeng ZW, et al. A novel NF-kappaB regulator encoded by circPLCE1 inhibits colorectal carcinoma progression by promoting RPS3 ubiquitin-dependent degradation. Mol Cancer. 2021;20:103.
42. Patel M, Horgan PG, McMillan DC, Edwards J. NF-kappaB pathways in the development and progression of colorectal cancer. Transl Res. 2018;197:43–56.
43. Wang S, Liu Z, Wang L, Zhang X. NF-kappaB signaling pathway, inflammation and colorectal cancer. Cell Mol Immunol. 2009;6:327–34.
44. Vaiopoulos AG, Athanasoula K, Papavassiliou AG. NF-kappaB in colorectal cancer. J Mol Med (Berl). 2013;91:1029–37.
45. Kojima M, Morisaki T, Sasaki N, Nakano K, Mibu R, Tanaka M, et al. Increased nuclear factor-kB activation in human colorectal carcinoma and its correlation with tumor progression. Anticancer Res. 2004;24:675–81.
46. Moorchung N, Kunwar S, Ahmed KW. An evaluation of nuclear factor kappa B expression in colorectal carcinoma: an analysis of 50 cases. J Cancer Res Ther. 2014;10:631–5.
47. Irving GR, Iwuji CO, Morgan B, Berry DP, Steward WP, Thomas A, et al. Combining curcumin (C3-complex, Sabinsa) with standard care FOLFOX chemotherapy in patients with inoperable colorectal cancer (CUFOX): study protocol for a randomised control trial. Trials. 2015;16:110.
48. Caponigro F, Lacombe D, Twelves C, Bauer J, Govaerts AS, Marreaud S, et al. An EORTC phase I study of Bortezomib in combination with oxaliplatin, leucovorin and 5-fluorouracil in patients with advanced colorectal cancer. Eur J Cancer. 2009;45:48–55.
49. Zhang Z, Li J, Huang Y, Peng W, Qian W, Gu J, et al. Upregulated miR-1258 regulates cell cycle and inhibits cell proliferation by directly targeting E2F8 in CRC. Cell Prolif. 2018;51:e12505.
50. Peng C, Tan Y, Yang P, Jin K, Zhang C, Peng W, et al. Circ-GALNT16 restrains colorectal cancer progression by enhancing the SUMOylation of hnRNPK. J Exp Clin Cancer Res. 2021;40:272.
51. Li J, Peng W, Yang P, Chen R, Gu Q, Qian W, et al. MicroRNA-1224-5p inhibits metastasis and epithelial-mesenchymal transition in colorectal cancer by targeting SP1-mediated NF-kappaB signaling pathways. Front Oncol. 2020;10:294.